Journal of Statistical Physics, Vol. 64, Nos. 5/6, 1991

The Role of Defects in the Transition Between Different Symmetries in Convective Patterns

S. Ciliberto,[1] E. Pampaloni,[1] and C. Perez-Garcia[2]

The properties of the transition between two patterns with different symmetries are studied in an experiment on thermal convection in a fluid layer heated from below. The defect structure is also analyzed and it is found that the unstable phase is present in the defect cores. The experimental results are in agreement with a model of three coupled Ginzburg–Landau equations.

KEY WORDS: Rayleigh–Bénard convection; patterns; defects; Ginzburg–Landau equation.

1. INTRODUCTION

Periodic spatial patterns appear in many biological, chemical, and physical systems; the analysis of their stability is a subject of great current interest. For example, it is important to investigate the structure of defects, the stability of the different symmetries, the influence of finite size, and whether it is possible to construct simple models that account for the experimental results.

One of the simplest pattern-forming systems in which the above-mentioned features can be studied is thermal convection in a horizontal fluid layer heated from below, that is, Rayleigh–Bénard convection. On a laboratory scale this fluid instability is very useful, because it is rather simple, in the experimental design, to take into account all the boundary conditions. In this paper we describe an example, concerning the transition from a structure of rolls to a hexagonal one in convective patterns. Specifically, we have studied the finite-size effects and the role of defects in this transition. It is important to point out that many of our findings are not

[1] Istituto Nazionale Ottica, 6-50125 Firenze, Italy.
[2] Departemento de Fisica, Universidad de Navarra, 31080 Pamplona, Navarra, Spain.

0022-4715/91/0900-1045$06.50/0

specific to the system under study, but are rather general, because they are explained by topological arguments based on the symmetries of the problem. The general properties of Rayleigh–Bénard convection may be found in standard textbooks and in review papers,[1] and thus we briefly mention, in Section 2, only the main features of this instability.

The rest of the paper is organized as follows. In Section 3 the experimental apparatus and the detection techniques are described. In Section 4 the transition between patterns with different symmetries is discussed. Section 5 is dedicated to the analysis of the defect structure. Finally, conclusions are presented in Section 6.

2. RAYLEIGH–BÉNARD CONVECTION

Rayleigh–Bénard convection is a fundamental mechanism of many natural phenomena, such as the mixing of water in the oceans, the movement of air in the earth's atmosphere, and the conduction of heat in stars. There are also many industrial applications. The cooling of big power plants is an example, in which the knowledge of convection properties is very important in order to increase the efficiency of the heat exchange processes. To illustrate the general features of Rayleigh–Bénard convection, let us consider a fluid layer confined between two horizontal solid plates and heated from below. The most relevant parameter of this instability is the Rayleigh number $R_a = \beta g \Delta T d^3/\nu\chi$, where β is the volumetric expansion coefficient, g the acceleration of gravity, ν the kinematic viscosity, χ the thermal diffusion coefficient, d the depth of the layer, and ΔT the difference of temperature between the two horizontal plates. When R_a exceeds the threshold value R_c a steady convective flow arises, producing a pattern of parallel rolls with a well-defined wavenumber q; a schematic view of this pattern is given in Fig. 1. The values of R_c and q depend on the sizes of the cell and on the

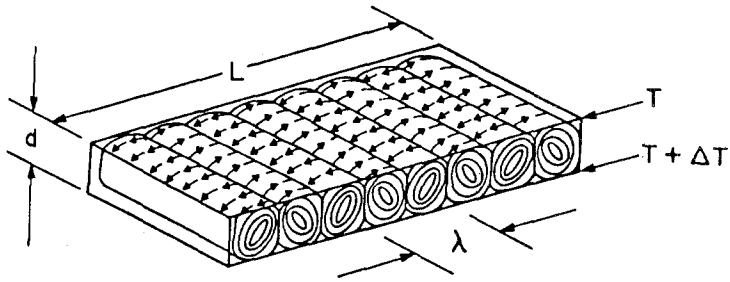

Fig. 1. Schematic drawing of convective pattern near R_c. The characteristic wavelength $\lambda = 2\pi/q$ is indicated.

nature of boundary conditions; for example, in the case of an infinite layer and perfect conducting plates $R_c = 1708$ and $q = 3.11/d$. Thus, from an experimental point of view, it is very important to define another parameter, the aspect ratio $\Gamma = L/d$, where L is the horizontal length of the cell. When $\Gamma \gg 2\pi/q$ the system has many spatial periods and the stability of periodic patterns may be studied near the convective threshold. The convective heat flow is strongly influenced by the presence of the walls, which have the effect of damping the fluid motion and thus of influencing the convective thresholds.

3. EXPERIMENTAL APPARATUS

A schematic cross section of a typical cell in which Rayleigh–Bénard convection is studied is reported in Fig. 2. The lateral walls of the cell are made of plexiglass. By changing the geometry and the sizes of the lateral walls it is possible to study the convective motion with different aspect ratios and boundary conditions. The bottom of the cell is a copper plate (CP) whose upper surface is finished to a mirror quality and is protected with a film of nickel to prevent oxidation. This plate is heated with an electrical resistor (ER). The upper plate is made of a sapphire window (SP)

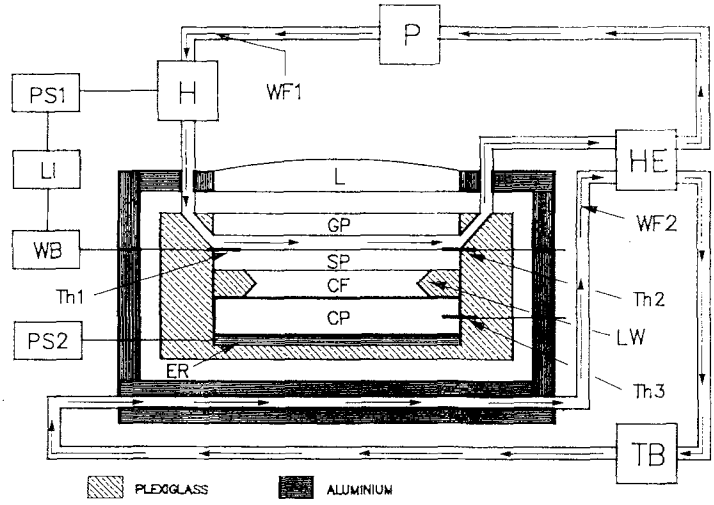

Fig. 2. Schematic diagram of the cell and of the thermal regulation system: CF, convective fluid; CP, copper plate; ER, electrical resistor; GP, glass plate; H, heater; HE, heat exchanger; L, lens; LI, lock-in amplifier; LW, lateral wall; P, pump; PS1(2), Power supplies; SP, sapphire plate; TB, thermal bath; Th1 (2, 3), thermistor 1 (2, 3); WB, Wheastone bridge; WF1 (2), water flows.

whose top is cooled by the water circulation (WF1), which is confined on the other side by the glass window (GP). This arrangement allows an optical investigation of the convective motion. The cell is inside a temperature-stabilized box that reduces the thermal fluctuations of the environment. The temperature of the cooling water WF1 is stabilized by a thermal bath and a feedback loop that controls the temperature of the upper plate. The long-term stability of ΔT is $\pm 0.005°C$. More details can be found in ref. 2.

The qualitative features of the patterns are determined by a digitally enhanced shadowgraph technique.[3] An optical technique, based on the deflection of a laser beam that sweeps the fluid layer,[2,4] enable us to obtain quantitative global and local characteristics of the pattern. The shadowgraph and laser beam deflection techniques are not perturbative and rely upon the changes of the index of refraction induced by the temperature field. The principle of the sweeping technique has been described elsewhere.[4] It allows us to measure the two components, averaged on the vertical direction, of the horizontal temperature gradient, produced by the convective motion. The temperature field can be simply restored by integration.

4. AN EXAMPLE OF PATTERN FORMATION

In the previous section it has been explained that, near the convective threshold, the fluid motion forms a pattern of rolls. This is true only in the cases in which the temperature dependence of fluid parameters can be neglected (Boussinesq conditions). On the other hand, when this dependence is important the pattern near threshold is composed of hexagons.[5,6] However, with increasing ΔT, hexagons become unstable and are replaced by rolls. Thus, convection, in this particular regime, may be used as a very simple pattern-forming system in which the transition between two different symmetries may be studied.[2,7,8] The system is a shallow horizontal layer of pure water heated from below. The layer of depth $d = 0.18$ cm is confined in a cylindrical cell of aspect ratio $\Gamma = r/d = 20$, where $r = 3.6$ cm is the radius of the cylinder. The experiment has been performed at the mean working temperature of 28.3°C, where the Prandtl number of water is 5.62 and the horizontal thermal diffusion time is $\tau_h = 2.45$ hours.[2] The convective motion appears when the temperature difference ΔT between the two horizontal plates is equal to $\Delta T_c = 12.62°C$. With such a big ΔT_c the temperature dependence of the transport coefficients cannot be neglected (non-Boussinesq conditions) and, therefore, a hexagonal pattern is formed near the convective threshold.[5] When $\varepsilon = (1 - \Delta T/\Delta T_c)$ is increased to $\varepsilon = \varepsilon_h = 0.09$ the hexagonal pattern is replaced by a pattern of rolls. Conversely, the roll–hexagon transition

occurs at $\varepsilon = \varepsilon_r = 0.03$ when ΔT is decreased. As an example, we show in Figs. 3a and 3b the shadowgraph images of two typical patterns. White and dark areas correspond to cold and hot fluid, respectively.

We see that at $\varepsilon = 0.02$ (Fig. 3a) a very regular pattern of hexagons is present, whereas at $\varepsilon = 0.14$ (Fig. 3b) the rolls are already formed. The transition from hexagons to rolls and vice versa is quantitatively characterized by studying the temperature field $T(x, y)$ measured with the laser sweeping technique mentioned in Section 3 on an array of 128×128 points on a square area of 4.9×4.9 cm^2.

In Fig. 4 we report the isotherms in a small central area of the cell, for three different values of ε. The corresponding Fourier spectra $S(K_x, K_y)$ of $T(x, y)$, computed in the full scanning area, are also shown. We see that the rolls slowly invade the hexagonal pattern, coming from the walls (not seen in Fig. 4, but observable in Fig. 3) where the perpendicular rolls behave like a seed of nucleation. Furthermore, we see that the amplitude of the peaks in the Fourier spectra changes during the transition. Thus, this amplitude is a good parameter to quantitatively characterize the transition. In looking at the spectra, one understands that the hexagonal pattern is composed of the sum of three sets of rolls. Each of them makes an angle $2\pi/3$ with both of the others. It can be shown that also the heat flow can be measured from the peak amplitudes. Specifically, the dimensionless heat flow is

$$\mathcal{N} = (N-1)\, R/R_c = \sum_k |\Psi_k|^2 \tag{1}$$

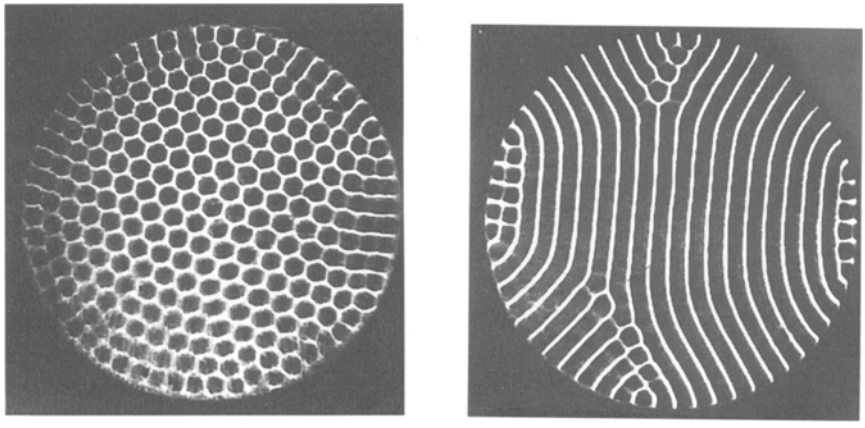

(a) (b)

Fig. 3. Shadowgraph images of two typical spatial patterns recorded at (a) $\varepsilon = 0.02$ and (b) $\varepsilon = 0.14$. White area corresponds to cold fluid going down, dark area to hot fluid rising up.

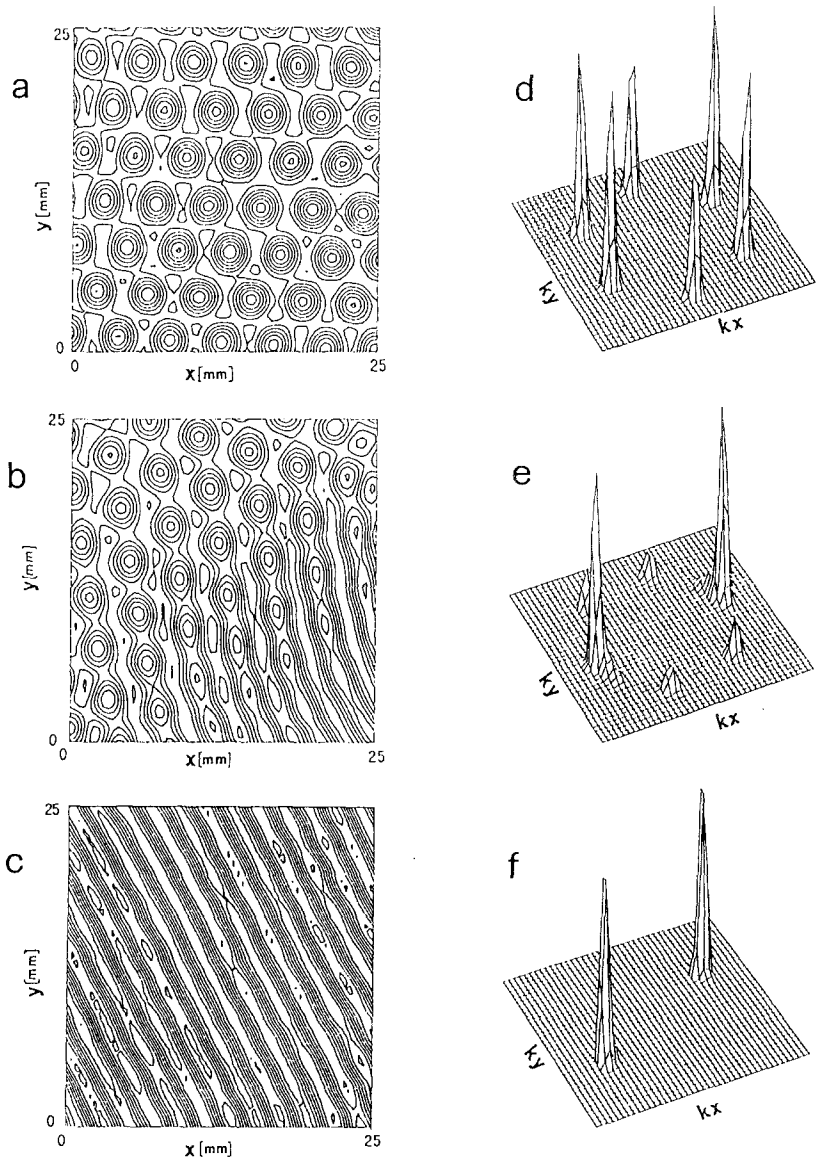

Fig. 4. Isotherms of the temperature field $T(x, y)$, for increasing ε in a small central area of the cell (δT is the temperature difference between two isotherms): (a) $\varepsilon = 0.022$ ($\delta T = 0.21°C$); (b) $\varepsilon = 0.041$ ($\delta T = 0.32°C$); (c) $\varepsilon = 0.110$ ($\delta T = 0.43°C$). (d–f) Fourier spectra of the temperature field in the full scanning area for the same values of ε as in (a–c), respectively.

where N denotes the Nusselt number, equal to the ratio between the total heat flow and the conductive heat flow (N is 1 when there is no convection). The Ψ_k are the dimensionless amplitudes of the Fourier modes of the temperature field, that is,

$$T(x, y) = \alpha_n \sum_k \Psi_k \exp(i\mathbf{K} \cdot \mathbf{r}) \tag{2}$$

where α_n is a suitable normalization factor introduced to satisfy Eq. (1). It may be computed from the theoretical analysis of refs. 8 and 9. In Fig. 4 we have seen that the peaks in the temperature Fourier spectrum are very sharp. Thus $T(x, y)$ can be decomposed into the sum of three main sets of rolls:

$$T(x, y) = \alpha_n \sum_{j=1}^{3} A_j(x, y) \exp(i\mathbf{K}_j \cdot \mathbf{r}) + \text{c.c.} \tag{3}$$

where the wavevectors $\mathbf{K}_j$ have the modulus equal to the critical wavevector K_c and $\sum_{j=1}^{3} \mathbf{K}_j = 0$. The heat flow is simply

$$\mathcal{N} = (N-1)\, R/R_c = \sum_{j=1}^{3} \langle |A|_j^2 \rangle_{x, y} \tag{4}$$

where $\langle \cdots \rangle_{x, y}$ means spatial average.

To obtain the amplitudes A_j we first compute the Fourier transform $F(K_x, K_y)$ of $T(x, y)$. The Fourier spectrum $S(K_x, K_y) = |F|^2$ presents six peaks (Figs. 4), whose centers of mass are at the vertices of the vectors $\mathbf{K}_j$ and $-\mathbf{K}_j$. These vectors are disposed on a hexagon in Fourier space (Fig. 4). Once the $\mathbf{K}_j$ are determined, we consider first the peak 1 and we shift $F(K_x, K_y)$ of $-\mathbf{K}_1$; thus, the peak 1 is centered in the origin. We filter out the contributions of all the other peaks by multiplying the shifted $F(K_x, K_y)$ by a low-pass filtering function (Hamming window)[10] having a suitable cutoff in the range of the peak width. Finally, we take the inverse Fourier transform to get the complex amplitude $A_1(x, y)$ of the first set of rolls. We repeat the same procedure (shift of $-\mathbf{K}_j$, low-pass filtering, and inverse transforms) for the two other sets of rolls. An easy calculation yields the real amplitude R_j as well as the phase φ_j for the three sets of rolls of the hexagonal pattern. The phases must satisfy the following equation: $\sum_{j=1}^{3} \varphi_j = 0$.

The competition between hexagons and rolls can be described by means of three coupled Ginzburg–Landau (GL) equations which determine the behavior of the three complex amplitudes A_i of the sets of rolls

describing the hexagonal structure. In the limit of homogeneous patterns these equations take the following form[6]:

$$\partial_t A_1 = \varepsilon A_1 + a A_2^* A_3^* - c\,|A_1|^2 A_1 - b(|A_2|^2 + |A_3|^2) A_1 \tag{5a}$$

$$\partial_t A_2 = \varepsilon A_2 + a A_1^* A_3^* - c\,|A_2|^2 A_2 - b(|A_1|^2 + |A_3|^2) A_2 \tag{5b}$$

$$\partial_t A_3 = \varepsilon A_3 + a A_2^* A_1^* - c\,|A_3|^2 A_3 - b(|A_1|^2 + |A_2|^2) A_3 \tag{5c}$$

where A^* denotes complex conjugate. In writing Eq. (5) the diffusive term $[\partial_x - (i/2K_c)\,\partial_y^2]^2$ has been neglected because it is irrelevant for the following discussion. The stationary solutions of Eqs. (5) are: (i) $A_r = A_1 \neq 0$ and $A_2 = A_3 = 0$ (rolls); (ii) $A_h = A_1 = A_2 = A_3 \neq 0$ (hexagons). The result of a linear stability analysis of these solutions is that rolls are stable for

$$\varepsilon > \varepsilon_r = \frac{a^2 c}{(b-c)^2} \tag{6}$$

hexagons are stable for $\varepsilon_a < \varepsilon < \varepsilon_h$, where

$$\varepsilon_a = \frac{-a^2 c}{4(2b+c)} \tag{7}$$

$$\varepsilon_h = \frac{a^2(b+2c)}{(b-c)^2} \tag{8}$$

and the ratio between the two threshold ε_h, ε_r is

$$\frac{\varepsilon_h}{\varepsilon_r} = \frac{b+2c}{c} \tag{9}$$

The coefficient a, b, c can be obtained by a best fit of the heat flow measurements. Specifically, for the hexagons the convective heat flow is

$$\mathcal{N}_h = 3\,|A_h|^2 = \frac{3}{C}\left[\frac{a^2}{2C} + \varepsilon + \frac{a}{2C}(a^2 + 4C\varepsilon)^{1/2}\right] \tag{10}$$

where $C = c + 2b$. For rolls

$$\mathcal{N}_r = |A_r|^2 = \frac{\varepsilon}{c} \tag{11}$$

As a consequence, the slope of the heat flow gives direct information about the coefficient c. The same coefficient can be obtained also by the theoretical analysis of Busse.[5]

The dependence of the heat flow measurements as a function of ε is shown in Fig. 5a. We observe that there are two regions, one for hexagons with $0.0 < \varepsilon < 0.04$ and one for rolls with $0.04 < \varepsilon < 0.14$. The continuous lines are the best fits obtained from Eqns. (10), (11). The slopes of the linear parts of these curves are $1/c = \gamma_r = 1.13 \pm 0.02$ for the rolls and $3/C = \gamma_h = 0.86 \pm 0.02$ and they are both smaller than those computed by Busse[5] for an infinite layer. The ratio $\gamma_r/\gamma_h = 1.30 \pm 0.05$ is instead in perfect agreement with theory. Thus the lateral walls have the effect of suppressing the convective motion and introduce a multiplicative factor that decreases the heat transport efficiency in the same way for hexagons and rolls.

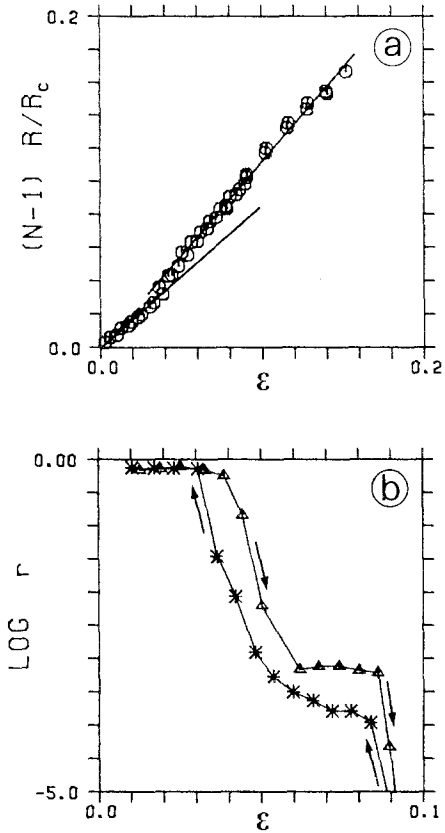

Fig. 5. (a) Dimensionless convective heat flow N. (b) Normalized ratio r (see text for details) as a function of ε. The arrows indicate the different evolutions of the vanishing modes when ε increases or decreases.

In order to characterize quantitatively the transition thresholds, we also define the ratio r:

$$r = \frac{\langle |A_2|^2 \rangle_{x,y} + \langle |A_3|^2 \rangle_{x,y}}{2\langle |A_1|^2 \rangle_{x,y}} \tag{12}$$

where A_1 is the amplitude of the surviving set of roll, while A_2, A_3 are the modes which disappear in the transition. In Fig. 5c the ratio r is plotted as a function of ε. The high plateau $r \simeq 1$ corresponds to hexagons, while the transition to a pattern of rolls is characterized as the limit $r \to 0$. From this figure one can deduce that a transition from hexagons to rolls (vanishing of two amplitudes) occurs between $\varepsilon_r = (3.0 \pm 0.1) \times 10^{-2}$ and $\varepsilon_h = (9.0 \pm 0.5) \times 10^{-2}$. These transition values are lower than those computed theoretically for an infinite system. However, the ratio $\varepsilon_h/\varepsilon_r = 3.0 \pm 0.27$ is slightly smaller than the theoretical value 3.44. The transition thresholds are smaller because the defects, whose core contains the unstable phase (see next section), act as seeds of nucleation for the other phase. It is important to point out that the appearence of defects is favored by the lateral walls. Thus, also the discrepancies between the theoretical and experimental thresholds can be seen as a consequence of the finite-size effects.

However, the transition thresholds and their ratio may be computed from Eqs. (6)–(8) once the coefficients a, b, c are known by the best fits of the heat flow measurements. We obtain $a = 8.63 \times 10^{-2}$, $b = 1.3 \pm 0.06$, and $c = 0.89 \pm 0.02$ and from Eq. (9), $\varepsilon_h/\varepsilon_r = 3.45 \pm 0.09$. This value is in perfect agreement with the ratio computed theoretically,[5] thus indicating that it is not affected by the finite-size effects. From Eqs. (6) and (8) we find that the thresholds computed are equal within error bars to the measured ones. The main conclusion is that the system (5) of three coupled Ginzburg–Landau equations is a good model for this transition. Moreover, this phenomenological procedure with which we have computed the transition thresholds allows us to correct the discrepancies, due to finite-size effects, between the theory of Busse[5] (valid for an infinite layer) and the experiment.

5. THE DEFECTS

A qualitative description of the cores of the various defects, which may be observed in this problem, can be deduced[11] from an elementary study of the nonlinear coupling existing among the modes in Eqs. (5).

When a hexagonal pattern is developed, the stationary defects observed in experiments consist of pairs of pentagonal–heptagonal cells, which

corresponds to having a roll in the defect core (punctual defect), as we will show in the next paragraph. Instead the grain boundaries are the defects of the roll patterns and they are produced by the junction of sets of rolls with different orientations. The hexagonal phase is found in the defect core (linear defect). In our experiment[2] no penta–hepta pairs were obtained spontaneously. In order to analyze this kind of defect, a penta–hepta pair is induced in some point of the convective pattern by means of some extra heating, obtained by focusing the light from a powerful lamp. Once this defect is induced it remains without variations for a very long time, sufficient to make measurements.

In Fig. 6a we report the isotherms of $T(x, y)$ at $\varepsilon = 0.02$; only a small portion of the cell is shown in order to amplify the details. The penta–heptha pair is easily observable in the center of the plot (Fig. 6a). In Figs. 6c and 6d the two phases φ_1, φ_3 are shown. We notice that in the core of the defect, i.e., in the common side of penta–hepta cells, φ_1 has a gap of $+2\pi$ around the core of the defect. The phase φ_3 has instead no singularity. The phase φ_2, of the third mode, has the same behavior as φ_1, but has a jump of -2π; as a consequence it is confirmed that the sum Φ of the three phases is zero also in the defect. The jump of $\pm 2\pi$ in the phases of two sets of rolls indicates that there is a dislocation in each of the two sets of rolls 1 and 2. This is confirmed by taking the amplitude R_j along some lines that cross the singularity (lines labeled with CS1 and CS2 in Fig. 6a). The results are shown in Figs. 6e and 6f, where one can see that, far from the defect, the three amplitudes are almost equal, i.e., they form a homogeneous hexagonal pattern. In contrast in the core of the penta–hepta pair, the two moduli R_1 and R_2 go to zero, whereas the third one R_3 increases locally in this region. This means that, locally, one has a pure roll in the core of the defect, i.e., the unstable solution appears in the defect of the stable solution.

On the other hand, when the pattern of rolls is well developed, some grain boundaries with a local hexagonal structure are observed (this defect is very stable and remains without variation for more than $140\tau_h$). The set of rolls in this experiment is always rather regular in the center of the cell. There are only a few grain boundaries produced by the readjustment of the rolls in the cylindrical container. We analyze now the core of one of these grain boundaries. The isotherms around it are reported in Fig. 7a; as in Fig. 6a, only a small portion of the cell is shown. This defect looks like a dislocation, but we will show that, in agrement with the above topological arguments, it is a grain boundary.

Here we may divide Fig. 7a into an upper and a lower part. In the former we see that there is a regular set of rolls almost parallel to the y direction; let us call the slowly varying amplitude of this set of rolls A_0. [It is

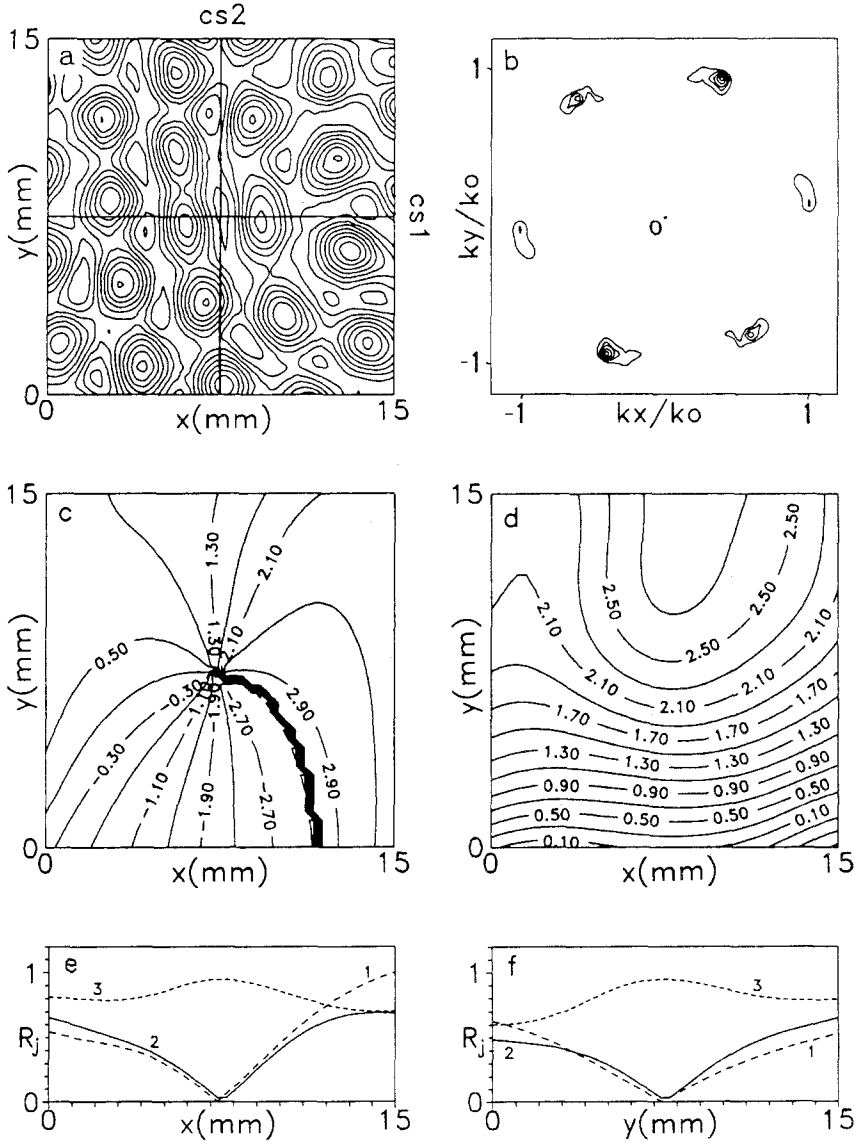

Fig. 6. Defect in a pattern of hexagons: Penta–hepta pair. (a) Isotherms of the convective temperature field $T(x, y)$ in a small area of the cell at $\mu = 0.02$. (b) Spatial Fourier spectrum of the field of (a). (c) Equiphase lines of φ_1. (d) Equiphase lines of φ_3. (e) Cross sections of the amplitudes R_j with $j = 1, 3$ along the line labeled CS1 in Fig. (3a). (f) As in (e), but the cross sections are done along CS2 in (a).

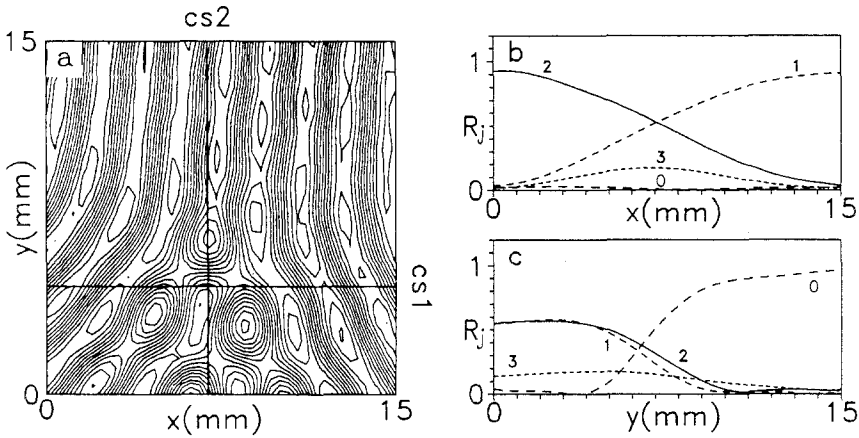

Fig. 7. Defect in a pattern of rolls: grain boundary. (a) Isotherms of the convective temperature field $T(x, y)$ in a small area of the cell at $\mu = 0.15$. (b) Cross sections of the amplitudes R_j, with $j = 0, 3$, along the line labeled CS1 in (a). (c) As in (b), but the cross sections are done along line labeled CS2 in (a).

important to notice that, in the case of a grain boundary, a systems of equations, equal to Eqs. (5), has to be considered for each of the sets of rolls contributing to the formation of the defect.] Instead in the lower part of Fig. 7a we have two other sets of rolls, one on the right, whose amplitude is A_1, and one on the left with amplitude A_2. They join with the main set of rolls and form an angle of about $\pi/3$ between them. By taking the Fourier spectrum of the pattern of Fig. 7a, we notice the presence of eight peaks, indicating the existence of another set of rolls (labeled with 3) not observable in Fig. 3a. This last set of rolls forms an angle of $\pi/3$ with the sets 1 and 2. The sets of rolls 1, 2, and 3 form a grain boundary, which is a typical defect of a system where there is a hexagon–roll competition.

We use the same procedure as in the penta–hepta pair to obtain the slowly varying amplitudes R_j and phases φ_j (with $j = 0, 3$) of the four modes present in this pattern. In Figs. 6b and 6c we show the amplitudes of the modes along the lines labeled CS1 and CS2 in Fig. 7a. From Figs. 7b and 7c one concludes that the amplitude R_0 of the main set of rolls goes to zero in the defect region; thus, it does not give any contribution to the defect formation. The amplitude R_1 (R_2) has a maximum where R_2 (R_1) has a minimum. In the core of the grain boundary where the two sets 1 and 2 interpenetrate, the amplitude R_3 reaches its maximum, which is smaller than those of the two oblique ones. Therefore, at the core of this typical defect in a pattern of rolls, the hexagonal unstable solution is encountered. Furthermore, the phases do not present any singularity. This fact confirms that there are no dislocations in the four sets of rolls.

6. CONCLUSION

We have shown that Rayleigh–Bénard convection under non-Boussinesq conditions is a simple system where the hexagon–roll competition may be investigated. By using optical methods we have studied in detail the transition properties and the defect structures. All the experimental results can be explained with a simple mathematical model of three coupled Ginzburg–Landau equations. This system of equations explains also that the unstable solution appears in the core of defects. The penta–hepta pair can be seen locally as a roll, and a grain boundary between two oblique rolls gives rise locally to hexagons. These defects play an important role in the dynamics of the transition between these two symmetries because they become seeds of nucleation for the other phase. It is important to stress that this is a completely general result because it is based on topological arguments on a system of coupled GL equations.[11]

ACKNOWLEDGMENTS

We have benefited from discussions with P. Coullet and J. Lega. This work has been partially supported by the EEC twinning project under contract SC1-0035-C and by the Italy–Spain Integrated Action (46-1989).

REFERENCES

1. S. Chandrasekar, *Hydrodynamic and Hydromagnetic Stability* (Clarendon Press, Oxford, 1961); F. H. Busse, *Rep. Prog. Phys.* **41**:1929 (1978); Ch. Normand, Y. Pomeau, and M. Velarde, *Rev. Mod. Phys.* **49**:581 (1977).
2. S. Ciliberto, E. Pampaloni, and C. Perez-Garcia, *Phys. Rev. Lett.* (1988); E. Pampaloni, C. Perez-Garcia, L. Albavetti, and S. Ciliberto, *J. Fluid Mech.*, to be published.
3. W. Merzkirch, *Flow Visualisation* (Academic Press, New York, 1974).
4. S. Ciliberto, F. Francini, and F. Simonelli, *Opt. Commun.* **54**:381 (1985).
5. F. H. Busse, *J. Fluid Mech.* **30**:625 (1967); C. Perez-Garcia, E. Pampaloni, and S. Ciliberto, *Europhys. Lett.* **12**:51 (1990).
6. L. A. Segel, *J. Fluid Mech.* **21**:359 (1965).
7. R. P. Behringer and G. Ahlers, *J. Fluid Mech.* **125**:219 (1982); M. Dubois, P. Bergé, and J. E. Wesfreid, *J. Phys.* **39**:1253 (1978).
8. G. Ahlers, M. C. Cross, P. C. Hohenberg, and S. Safran, *J. Fluid Mech.* **110**:297 (1981).
9. M. C. Cross, *Phys. Fluids* **23**:1727 (1980).
10. A. V. Oppenheim and R. W. Schafer, *Digital Signal Processing* (Prentice-Hall, 1975); L. R. Rabiner and B. Gold, *Theory and Applications of Digital Signal Processing* (Prentice Hall 1974).
11. S. Ciliberto, P. Coullet, J. Lega, E. Pampaloni, and C. Carlos Perez Garcia, *Phys. Rev. Lett.* **65**:2370 (1990).